Painlevé IV with Both Parameters Zero: A Numerical Study

By Jonah A. Reeger [1] and Bengt Fornberg [2]

The six Painlevé equations were introduced over a century ago, motivated by rather theoretical considerations. Over the last several decades, these equations and their solutions, known as the Painlevé transcendents, have been found to play an increasingly central role in numerous areas of mathematical physics. Due to extensive dense pole fields in the complex plane, their numerical evaluation remained challenging until the recent introduction of a fast 'pole field solver' (Fornberg and Weideman, J. Comp. Phys. 230 (2011), 5957-5973). The fourth Painlevé equation has two free parameters in its coefficients, as well as two free initial conditions. The present study applies this new computational tool to the special case when both of its parameters are zero. We confirm existing analytic and asymptotic knowledge about the equation, and also explore solution regimes which have not been described in the previous literature.

Key words Painlevé equation, Painlevé transcendent, P_{IV}, pole field, connection formula.

1 Introduction

The six Painlevé equations (P_I-P_{VI}) are second order ordinary differential equations (ODEs) with solutions that are free from movable branch points, but with the possibility of movable poles or movable isolated essential singularities [1, Section 32.2]. The term movable refers to the dependence of their location on the ODE's initial data. The second through sixth

[1]Captain, United States Air Force, supported by the Department of Defense. The views expressed in this article are those of the authors and do not reflect the official policy or position of the United States Air Force, Department of Defense, or U.S. Government. Address for correspondence: University of Colorado, Department of Applied Mathematics, 526 UCB, Boulder, CO 80309 USA.

[2]Supported by NSF grant DMS-0914647. Address for correspondence: University of Colorado, Department of Applied Mathematics, 526 UCB, Boulder, CO 80309 USA.

Discussions with André Weideman are gratefully acknowledged.

Painlevé equations also exhibit dependence on one to four arbitrary parameters. The fourth Painlevé equation (P_{IV}),

$$\frac{d^2}{dz^2}u(z) = \frac{1}{2u(z)}\left(\frac{d}{dz}u(z)\right)^2 + \frac{3}{2}u(z)^3 + 4zu(z)^2 + 2\left(z^2-\alpha\right)u(z) + \frac{\beta}{u(z)}, \qquad (1)$$

has two such parameters, α and β. Together with two initial conditions (ICs) a vast array of solutions can arise.

The solutions to the Painlevé equations are often dubbed the Painlevé transcendents since, except for a very small subset of the possible parameter choices and ICs, they are not expressible in terms of elementary or traditional special functions. With regard to P_{IV}, a particularly small portion of the two-dimensional parameter space leads to solutions expressible as rational functions or in terms of special functions such as the parabolic cylinder function. These solutions are well documented; however, nearly all of the parameter and IC choices are unexplored. For the case $\alpha = \beta = 0$, which this study focuses on, no closed form solution is known (apart from the trivial $u(z) = 0$).

The growing importance of the Painlevé transcendents in mathematical physics is reflected in that they, although absent in the classical Handbook of Mathematical Functions [2], have received a full chapter in the NIST Handbook [1]. Numerous applications for the Painlevé equations are given in [1, Sections 32.13-32.16], along with extensive references. These include reductions of partial differential equations, combinatorics, and many physical applications including statistical and quantum physics. Some applications specific to the P_{IV} equation include random matrix theory (see, e.g., [3], [4], [5], and [6]) and supersymmetric quantum mechanics (e.g., [7]). Further applications are noted in [8].

The explorations we describe in this paper are mostly computational. Some early computational work on P_{IV} in [9] focused on the real line with little or no exploration into the complex plane. The numerical approach introduced in [10]–combining a Padé based ODE solver [11] with a partly randomized integration path strategy–allowed for the first time rapid numerical solutions of the Painlevé equations over extended regions in the complex plane. It was first used for P_I in [10] and later for P_{II} in [12]. This paper describes similar computations for P_{IV}.

1.1 Organization of the paper

This paper will first cover some background information about P_{IV}, such as the series expansion around a pole and a notable symmetry in the differential equation. The known asymptotic approximations are followed up with a discussion on computing corresponding ICs. Verifications of these asymptotic approximations and further numerical explorations are then considered, including solutions with a pole located at the origin.

2 Background Observations

2.1 Series Expansion

In a neighborhood of a pole z_0 the coefficients of the Laurent expansion of P_{IV} can be determined by substituting a truncated expansion

$$u(z) = \sum_{k=-1}^{n} a_k (z - z_0)^k + O((z - z_0)^{n+1}) \tag{2}$$

into (1) (starting with $k = -1$ since otherwise $a_k = 0$ for $k < -1$). For example, choosing $n = 4$ and equating coefficients gives

$$\begin{aligned}
a_{-1} &= \pm 1 \\
a_0 &= -z_0 \\
a_1 &= \frac{1}{3}(-4 \pm z_0^2 \pm 2\alpha) \\
a_2 &= c \\
a_3 &= \frac{1}{45}(\pm 26 \mp 36cz_0 + 20z_0^2 \mp z_0^4 - 32\alpha \mp 4z_0^2\alpha \pm 14\alpha^2 \pm 9\beta) \\
a_4 &= \frac{1}{9}(\mp 9c + 5z_0 + 3cz_0^2 \mp 2z_0^3 + 6c\alpha \mp 4z_0\alpha).
\end{aligned}$$

Hence, all poles in the solutions to P_{IV} are simple and have residue of either $+1$ or -1. The only further free parameter is c, first appearing in a_2.

2.2 Symmetry in the P_{IV} Equation

Let $P_{IV}(\alpha, \beta)$ be the set of all solutions of (1) for the particular α and β. Direct inspection of (1) shows that if $u(z) \in P_{IV}(\alpha, \beta)$, then

$$-u(-z) \in P_{IV}(\alpha, \beta), \tag{3}$$

$$-iu(iz) \in P_{IV}(-\alpha, \beta), \text{ and} \tag{4}$$

$$iu(-iz) \in P_{IV}(-\alpha, \beta) \text{ [13].} \tag{5}$$

Incidentally the first of these symmetries also holds for P_{III} (for all parameter choices), but never for any of the other Painlevé equations. With our current focus on $\alpha = \beta = 0$, we note in particular that if $u(z) \in P_{IV}(0, 0)$, then $-u(-z)$, $-iu(iz)$, and $iu(-iz) \in P_{IV}(0, 0)$. This first symmetry simplifies the analysis of the various computations considered in this paper. For instance, the number of poles and oscillations over a given interval of the real line is monitored to determine ICs that give pole- and/or oscillation-free solutions over the entire real line. When given initial data to the ODE at $z = 0$ it then suffices to consider the solution for an interval along the positive real axis. It is important to keep this symmetry in mind since any solution presented in this paper has a counterpart that is the odd reflection about the origin among others.

3 Asymptotic Approximations

Much of the previous computational work on P_{IV} was designed to verify its asymptotic approximations. A contributing factor to this was likely the difficulty experienced by typical ODE solvers when encountering a pole. For instance, solutions with very special parameter choices were explored in [9] using a classical fourth order Runge-Kutta scheme, a sixth-order scheme, and an Adams Moulton predictor-corrector method, each of which are rendered ineffective when encountering a pole. Alternate approaches that are applicable also when poles are encountered have been proposed in [14] and [15]. A wider selection of parameter choices will be discussed in the following subsections.

3.1 Parameter Choices, an Approximation, and Connection Formulae

Before limiting to the case of $\alpha = \beta = 0$, let $\alpha = 2\nu + 1 \in \mathbb{R}$ and $\beta = 0$ (with $\nu = -\frac{1}{2}$ giving $\alpha = 0$). Equation (1) then becomes

$$\frac{d^2}{dz^2}u(z) = \frac{1}{2u(z)}\left(\frac{d}{dz}u(z)\right)^2 + \frac{3}{2}u(z)^3 + 4zu(z)^2 + 2\left(z^2 - 2\nu - 1\right)u(z). \tag{6}$$

This particular form of P_{IV} is presented in [1, Section 32.11] and is in contrast to those presented in [9] and [16], where the change of variables

$$u(z) = 2\sqrt{2}w(x)^2 \text{ and } z = \frac{1}{2}\sqrt{2}x \tag{7}$$

is applied. For some of the following examples, the boundary condition

$$u(z) \to 0, \text{ as } z \to +\infty \text{ and } z \in \mathbb{R} \tag{8}$$

is also imposed. Based on the symmetry (3) discussed previously, the condition $u(z) \to 0$, as $z \to -\infty$ could likewise be considered, to achieve analogous results.

It is noted in the NIST handbook [1, Section 32.11(v)] that any nontrivial solution of (6) satisfying (8) is asymptotic to

$$k\left(D_\nu(\sqrt{2}z)\right)^2 \text{ as } z \to +\infty \text{ and } k \neq 0, \tag{9}$$

where $k \in \mathbb{R}$ and $D_\nu(\zeta)$ is the parabolic cylinder function, satisfying

$$\frac{d^2}{d\zeta^2}D_\nu(\zeta) = \left(\frac{1}{4}\zeta^2 - \nu - \frac{1}{2}\right)D_\nu(\zeta)$$

with boundary conditions

$$D_\nu(\zeta) \sim \zeta^\nu e^{-\frac{1}{4}\zeta^2},\ \zeta \to +\infty.$$

Previous studies of P_{IV} present only cases where $k > 0$; however, this study will also consider $k < 0$.

There is a critical value of k given by

$$k^* = \frac{1}{\sqrt{\pi}\Gamma(\nu+1)} \tag{10}$$

such that when $0 \leq k < k^*$ there are no poles on the real axis. In the case of $\nu = -\frac{1}{2}$, $k^* = \frac{1}{\pi}$.

One can further distinguish between two cases for ν when $0 \leq k < k^*$. First, if $\nu \in \mathbb{Z}^+$, then $u(z)$ is asymptotic to

$$k2^\nu z^{2\nu} e^{-z^2},\ z \to -\infty. \tag{11}$$

Likewise, if $0 \neq \nu \notin \mathbb{Z}^+$, which includes the present case of $\nu = -\frac{1}{2}$, then $u(z)$ is asymptotic to

$$-\frac{2}{3}z + \frac{4}{3}d\sqrt{3}\sin(\phi(z) - \theta_0) + O(z^{-1}),\ z \to -\infty, \tag{12}$$

where

$$\phi(z) = \frac{1}{3}\sqrt{3}z^2 - \frac{4}{3}d^2\sqrt{3}\ln(\sqrt{2}|z|). \tag{13}$$

Here d and θ_0 are given by the connection formulas, derived in [17], as

$$d^2 = -\frac{1}{4}\sqrt{3}\pi^{-1}\ln(1 - |\mu|^2) \tag{14}$$

and

$$\theta_0 = \frac{1}{3}d^2\sqrt{3}\ln(3) + \frac{2}{3}\pi\nu + \frac{7}{12}\pi + \arg(\mu) + \arg\left(\Gamma\left(-\frac{2}{3}i\sqrt{3}d^2\right)\right), \tag{15}$$

with

$$\mu = 1 + \frac{2ik\pi^{3/2}e^{-i\pi\nu}}{\Gamma(-\nu)}. \tag{16}$$

Note that the connection formulas for d and θ_0 were presented incorrectly in [18] and [19],

but corrected in, for example, [9] and [16].

Next, for $k = k^*$, $u(z)$ again has no poles on the real axis and is asymptotic to $-2z$ for $z \to -\infty$. Finally, if $k > k^*$ or $k < 0$, then $u(z)$ has poles on the real axis whose locations are dependent on k. Previous studies of P_{IV} do not explicitly describe the behavior of (6) with $k < 0$. Infinitely many poles are found along the negative real axis in these cases.

Applying the method of dominant balance (see, e.g., [20, Section 3.4]) to (6) leads to the asymptotic relation

$$u_{\pm}(z) \sim \frac{-4z \pm 2\sqrt{z^2 + 6\nu + 3}}{3} \text{ as } |z| \to \infty.$$

Taking $\nu = -\frac{1}{2}$ leads to $u_+(z) \sim -\frac{2}{3}z$ and $u_-(z) \sim -2z$, respectively, with the upper and lower sign choice. The dominance of this relation is apparent for $0 < k \leq k^*$; however, this approximation is not meaningful for $k > k^*$ or $k < 0$. It is particularly important in the cases of $k = k^*$ and $k = \frac{1}{2}k^*$, as we will show later.

3.2 Computing the ICs for Asymptotic Approximations

Consider the asymptotic condition (9), shown in the left of figure 1. The values of $(D_\nu(\sqrt{2}z))^2$ are less than machine precision for even relatively small values of z. As it will transpire, z can nevertheless be selected such that it is large enough to make the approximation useful and small enough so that a solution of (6) is computable to machine precision.

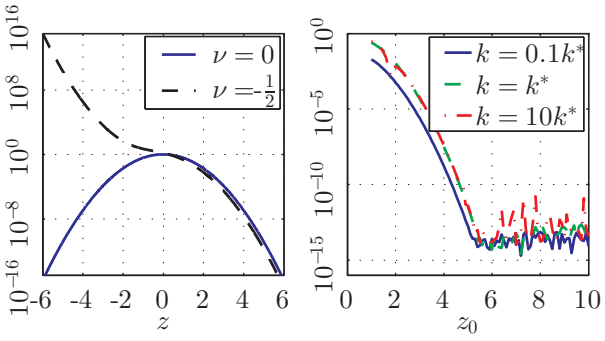

Figure 1: Left: A plot of $(D_\nu(\sqrt{2}z))^2$ with $k = 1$. Right: A plot of $\left|\frac{u(0)-\widehat{u}(0)}{u(0)}\right|$ for various values of k and $\nu = 0$. Roundoff begins to dominate the error in $\widehat{u}(0)$ when z_0 is slightly more than 5.

It is stated in [9] that, for $\nu = 0, 1, 2, \ldots$, a closed form solution to (6) for arbitrary values of k and $z \in \mathbb{R}$ exists. For instance, for $\nu = 0$ the solution becomes

$$u(z) = \frac{2\sqrt{2}k\exp(-z^2)}{2^{3/2} - k\sqrt{2\pi}\mathrm{erfc}(z)},$$

where

$$\mathrm{erfc}(\zeta) = \frac{2}{\sqrt{\pi}}\int_{\zeta}^{\infty}\exp(-s^2)ds$$

is the complementary error function discussed in [1, Section 7.2]. Knowing this closed form solution, the exact value of $u(0)$ can be compared to the value obtained numerically beginning with initial conditions

$$k\left(D_{\nu}(\sqrt{2}z_0)\right)^2, \tag{17}$$

$z_0 \in [1, 10]$. Call this numerical solution $\widehat{u}(0)$. Comparing the left and right images in figure 1 shows that for various k $z_0 \approx 5$ can be chosen to achieve an accurate solution with $(D_{\nu}(\sqrt{2}z_0))^2$ large enough. To be in agreement with the choice of z_0 to generate initial data in [9] $z_0 = 4\sqrt{2} \approx 5.65$ is used throughout this article, which has been shown to be sufficient.

In the case of the P_{II} equation,

$$\frac{d^2}{dz^2}u(z) \quad = \quad 2u(z)^3 + zu(z) + \alpha,$$

it was found in [12] that its leading asymptotic term alone was numerically sufficient when $\alpha = 0$, but otherwise needed to be supplemented by asymptotic expansions. We encounter the same situation with P_{IV} in its $\alpha = \beta = 0$ case. The leading term in

$$\begin{aligned} u(z) \quad \sim \quad & k\left(D_{-\frac{1}{2}}(\sqrt{2}z)\right)^2 + \\ & k^2\frac{e^{-2z^2}}{z^3}\left[\frac{1}{4} - \frac{9}{16}\frac{1}{z^2} + \frac{205}{128}\frac{1}{z^4} - + \cdots\right] + \\ & k^3\frac{e^{-3z^2}}{\sqrt{2}z^5}\left[\frac{1}{8} - \frac{31}{64}\frac{1}{z^2} + \frac{1853}{1024}\frac{1}{z^4} - + \cdots\right] + \\ & O\left(\frac{e^{-4z^2}}{z^7}\right). \end{aligned}$$

suffices for any choice of $z > 4$. Further terms are here unnecessary for the identification of critical k-values.

4 An Exploration of the $u(0)$, $u'(0)$-Plane

4.1 Pole and Oscillation Counting

A particularly useful tool in determining the various types of solutions that exist for fixed α and β is to count the number of poles and oscillations that occur in a given interval on either the positive or negative real axis. Displays can then be created that indicate the number of poles appearing on the positive or negative real axis for different regions of the $u(0)$, $u'(0)$ plane. This is shown in figure 2 for the case $\alpha = \beta = 0$ (that is, $\nu = -\frac{1}{2}$). The left and right images were produced by counting the number of poles to the left and right of the origin, respectively. The symmetry (3) is apparent in these figures.

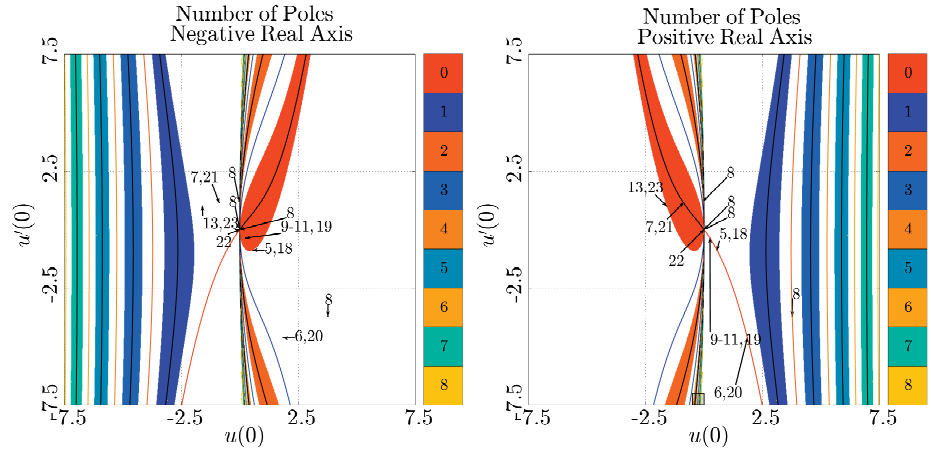

Figure 2: Number of poles on the negative (left) and positive (right) real axes. The colored regions correspond to solutions with a fixed number of poles on the appropriate half of the real axis; however, these solutions may have oscillations over that half. The black and colored curves indicate initial conditions with a fixed number of poles and no oscillations on the corresponding half of the real axis. White regions correspond to an infinity of poles. The area in the small box at the bottom of the right figure is enlarged in figure 3.

Consider, for now, only the right frame in figure 2, since the left is completely analo-

gous. Each of the ICs marked by a curve or contained within a shaded region generates a solution with a finite number of poles on the positive real axis. The color bar indicates the exact number of poles for a given initial condition with darker (blues/greens) and lighter (reds/yellows) indicating odd and even numbers of poles, respectively.

Each of the shaded regions in the right half-plane contains ICs that generate solutions with an odd number of poles on the positive real axis, while the $u(0)$, $u'(0)$ values along the colored curves lead to solutions with an even number. The left half-plane is the opposite.

Most of the ICs in the shaded regions generate solutions that oscillate as $z \to +\infty$; however, each initial condition marked by a curve or located at the boundary of a shaded region has no oscillations as $z \to +\infty$.

Figure 2 also identifies the initial conditions of many of the solutions shown in this paper by marking them with an arrow and the corresponding figure number(s).

Still focusing on the right frame, notice that as $u(0) \to 0$ from the left the shaded regions become finer. Figure 3 shows two zoomed windows to further highlight this behavior. In these images it is shown that these regions become infinitely narrower as $u(z)$ approaches zero and in each consecutive region the number of poles increases by two.

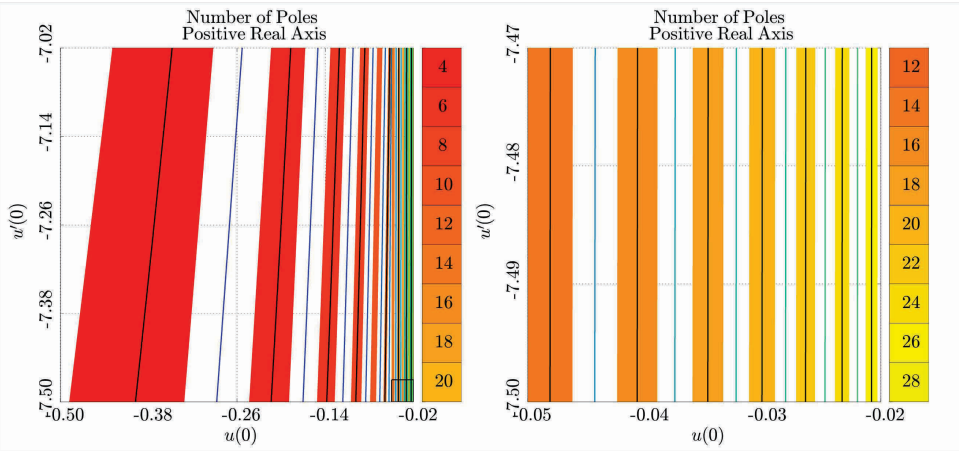

Figure 3: Zoomed views of the number of poles on the positive real line. The left frame corresponds to the box outlined in the right frame of figure 2 and the right frame corresponds to the box highlighted in the left frame of this figure. Note that the right edge corresponds to $u(0) = -0.02$, rather than $u(0) = 0$, to avoid displaying an infinity of shaded regions.

4.2 Exploring the Known Asymptotic Solutions

Armed with the pole- and oscillation-counting images, two natural questions become: "Which initial conditions correspond to varying k?" and "What do the solutions to these asymptotic approximations look like across the complex plane?"

To answer the first question k is varied from near zero to $|k| \gg 0$. The dashed and solid curves in figure 4 indicate the location of $u(0)$ and $u'(0)$ found by varying k and computing the numerical solution beginning with (17) at $z_0 = 4\sqrt{2}$. The continuation of the curves outside the axes illustrates the transitions of $u(0)$ and $u'(0)$ to $+\infty$ or $-\infty$ and back as we increase or decrease k. This is due to the movement of a pole through the origin $z = 0$. A following section will show that the continuation of the dashed and solid curves corresponds to a pole at the origin with positive and negative residue, respectively.

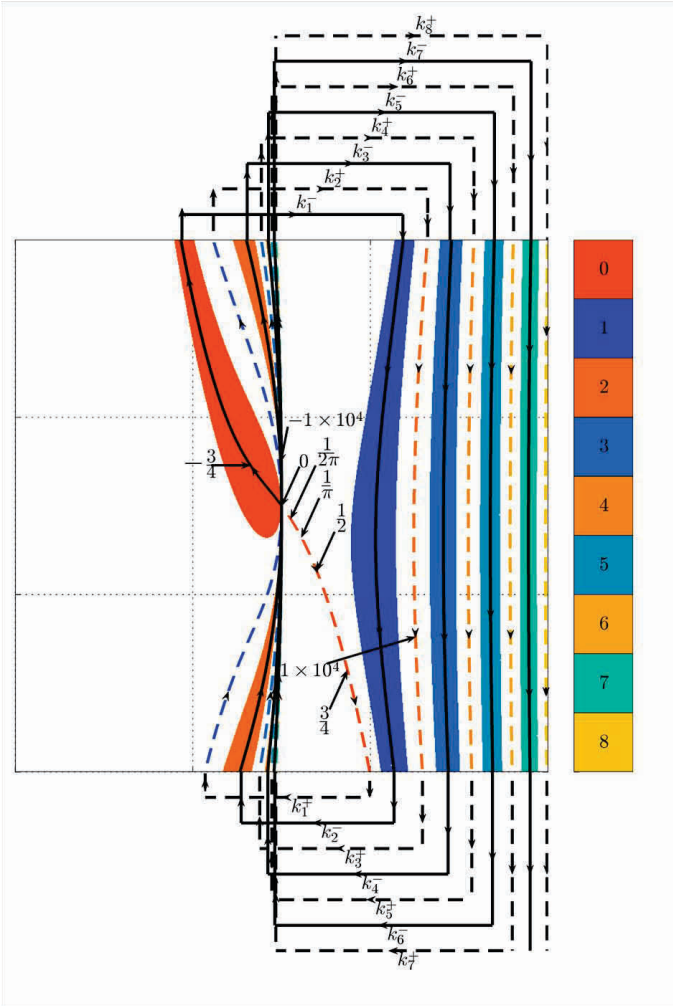

Figure 4: A view of how $u(0)$ and $u'(0)$ change as k is varied. The locations of several values of k are marked. The dashed and solid curves represent values when $k > 0$ and $k < 0$, respectively. The labels $k_j^{\pm}$, $j = 1, 2, \ldots, 8$, correspond to diffferent values of c in figures 15 and 16, which represent the movement of a pole through the origin. Approximate values of k and c are also shown in table 1. Note that this image is a detailed version of the right frame of figure 2, where the horizontal axis indicates the value of $u(0)$ from -7.5 to 7.5 and the vertical axis indicates the values of $u'(0)$, again from -7.5 to 7.5.

Next, the second question is answered with examples of the solutions similar to those presented (along the real axis) for the transformed case of P_{IV} in [1], [9] and [16]. To this end, a number of solutions are presented in a two frame format. The left frames display

the pole locations and corresponding residues, dark (blue) for +1 and light (yellow) for -1. The right frames display the solution along the real axis, in a style similar to figure 32.3.6 in [1] (but without stopping when a pole is encountered); that is, solutions are displayed for $k = k^* - 1 \times 10^{-8}$, $k = k^*$ and $k = k^* + 1 \times 10^{-8}$. Notice that for $0 < k \leq k^*$ there are no poles on the real axis and that the asymptotic approximations of $-2z$ and (12) match well even for z close to the origin.

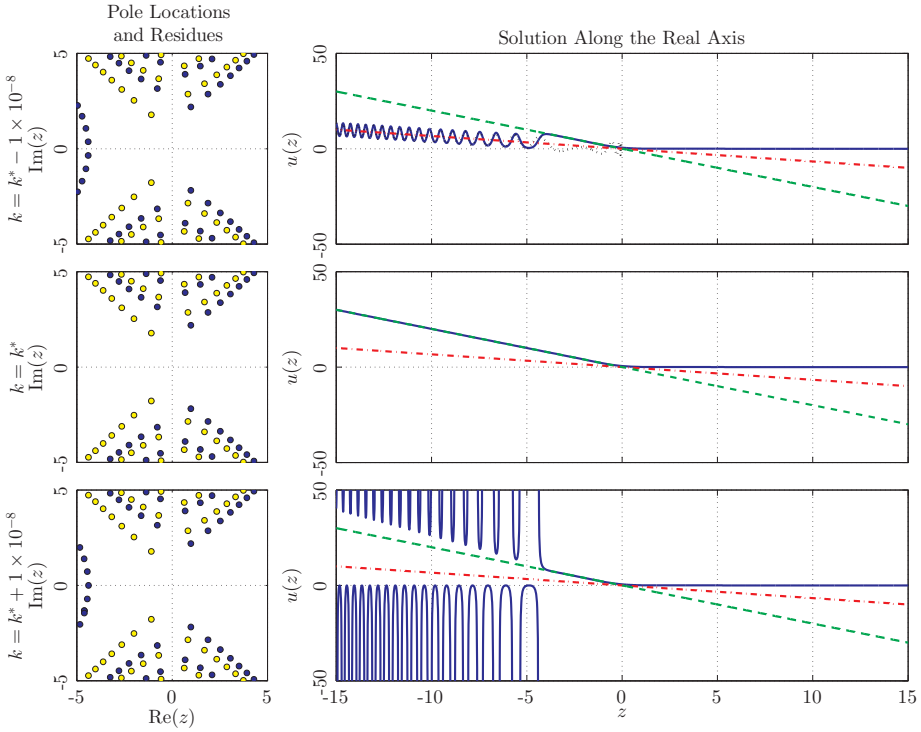

Figure 5: Solutions to (6) with $\nu = -\frac{1}{2}$. The solid (blue) lines indicate the numerical solutions. The dashed-dotted (red) and dashed (green) lines show $-\frac{2}{3}z$ and $-2z$, respectively. The dotted (black) lines in the first and second rows show (12).

Generally, the solutions of (6) satisfying (9) with $k > 0$ occur at critical initial data where a region of poles has moved out to infinity leaving a pole free region of the complex plane behind. For simplicity, refer to this type of solution as a k-positive solution. An example of this appears in figure 6, where the initial conditions for the middle row of frames are generated from (6) and (9) by choosing $k = +0.75$. The top and bottom rows show the

solutions in a neighborhood of the generated initial data.

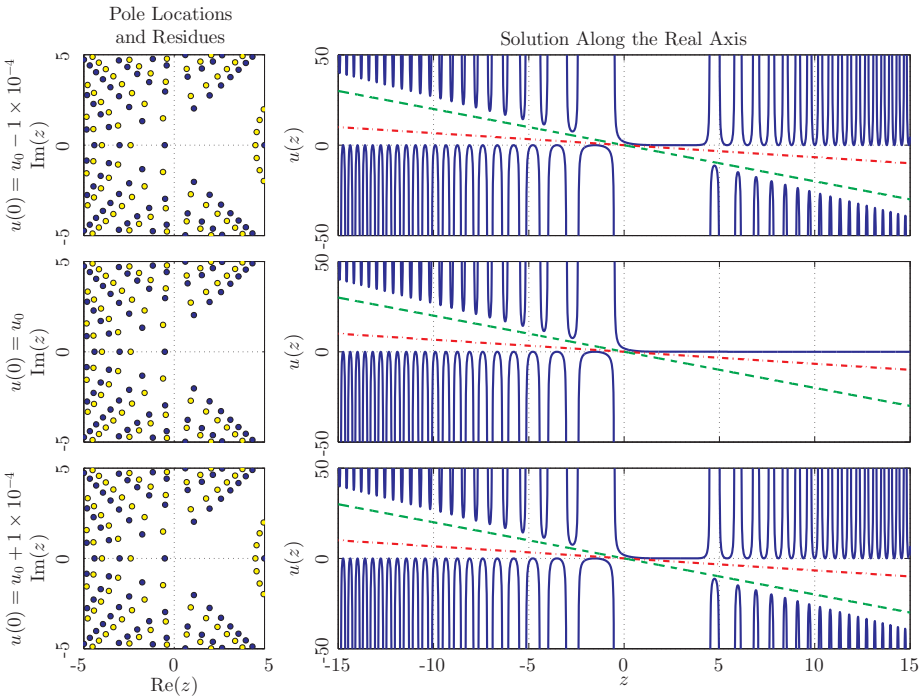

Figure 6: A view of the solutions that have poles that move to $+\infty$ leaving a near zero segment behind and then return. In all cases $u_0 = 1.84810583$ and $u'(0) = -4.61669536$, which result from integrating (6) ($\nu = -\frac{1}{2}$) starting with (9) ($k = 0.75$) from $z = 4\sqrt{2}$ to $z = 0$. There is no noticeable difference between the top and bottom figure sets, highlighting that there is no change in pole field orientation as we pass through these special ICs.

On the other hand, choosing $k < 0$ leads to another type of solution. As $u(0)$ and $u'(0)$ generated from (6) and (9) for $k < 0$ are approached the solutions have an infinity of oscillations that move toward $+\infty$ while leaving a near zero solution behind. These solutions will be referred to as k-negative solutions. Picking $k = -0.75$ the solution in the middle row of figure 7 is found. The top and bottom rows again highlight the movement of the oscillations for $u(0)$ and $u'(0)$ in a neighborhood of the generated initial data.

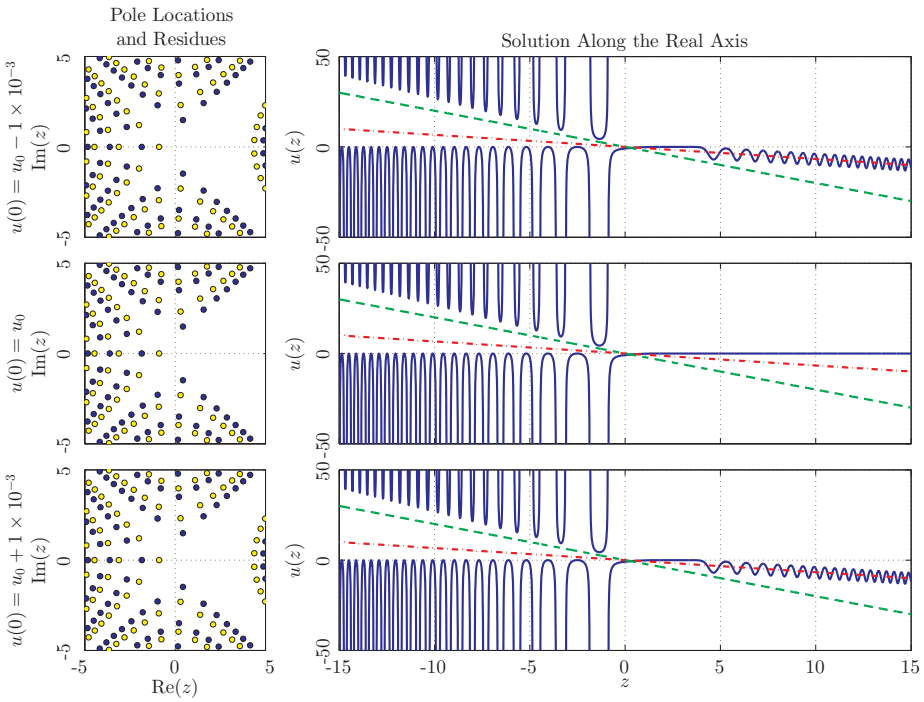

Figure 7: A view of the solutions that have oscillations that move to $+\infty$ leaving a near zero segment behind and then return. In all cases $u_0 = -0.87721765$ and $u'(0) = 1.14146647$, which result from integrating (6) ($\nu = -\frac{1}{2}$) starting with (9) ($k = -0.75$) from $z = 4\sqrt{2}$ to $z = 0$. There is no noticeable difference between the top and bottom figure sets, highlighting that there is no change in pole field orientation as we pass through these special ICs.

Figures 6 and 7 show another, yet peculiar, behavior of the solutions of the P_{IV} equation. As $u(0)$ and $u'(0)$ pass through critical ICs for both P_I and P_{II} there is a distinct change in the location of the poles closest to the real axis. For instance, let u_0 and u_0' be critical ICs for P_I and $u(0) = u_0 - \epsilon$ and $u'(0) = u_0'$ generate a solution with no poles on the negative real axis. Then the solution for $u(0) = u_0 + \epsilon$ and $u'(0) = u_0'$ will have an infinity of the poles on the negative real axis. An example of this is shown for P_I in figure 4.3 of [10], which is also shown only on the real axis in figure 32.3.3 of [1]. This same behavior has been witnessed for all possible choices of critical ICs shown in the available literature for P_{II}.

On the other hand, if $u(0)$ or $u'(0)$ generated from (6) and (9) are fixed and a small neighborhood of $u'(0)$ or $u(0)$, respectively, is considered, then there is no change in pole

field orientation or residue when passing through the critical ICs. The action of passing through the critical ICs is the same as passing through either a solid or dashed line in figure 4. This is the behavior for nearly all of the k-positive and k-negative solutions, except those which occur at the boundary of a shaded region in figure 4. An example of this appears in figure 5.

To complete this section consider extreme values of k. That is, consider values of k with very large and very small magnitudes. Figure 8 shows some such solutions.

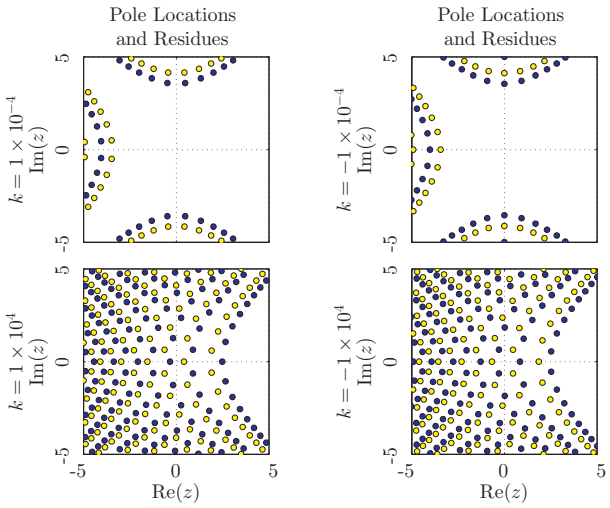

Figure 8: A view of the solutions which result from (6) starting with (9), where $\nu = -\frac{1}{2}$ and four different values for k.

Notice that values of k that are equal in magnitude but opposite in sign lead to solutions that are similar, but with the sign of the residue of the pole located furthest to the right on the real axis equalling the sign of k.

4.3 Solution with a Pole Free Half-Plane

One of the more interesting cases appears in figure 9, when $k = 0.5k^*$. In this case, the solution follows $-\frac{2}{3}z$, as $z \to -\infty$ and $z \in \mathbb{R}$, and appears pole and oscillation free across the entire real axis. In fact, (12) becomes $-\frac{2}{3}z$, and substitution of $u(z) = -\frac{2}{3}z$ into (6) with $\nu = -\frac{1}{2}$ leads to a residual of $\frac{1}{3z}$. Figure 10 shows a sequence of solutions where k increases to $\frac{1}{2}k^*$ and beyond. Notice that two regions of poles, nearly symmetric about the

rays $re^{\pm i\frac{3\pi}{4}}$, $r \geq 0$, move away from the origin and, after the critical $k = 0.5k^*$, return with changed orientation.

Figure 11 displays a sequence of frames of size 1×0.5 in the real and imaginary directions, respectively, depicting $|u(z)|$ adjacent to the imaginary axis. This frame size was chosen so that the magnitude of $u(z)$ could be clearly displayed when the density of the poles is so great near $\mathrm{Im}(z) = 100$. The distance of the nearest row of poles from the imaginary axis appears to be $O\left(\frac{1}{\mathrm{Im}(z)}\right)$, with the left half-plane pole free.

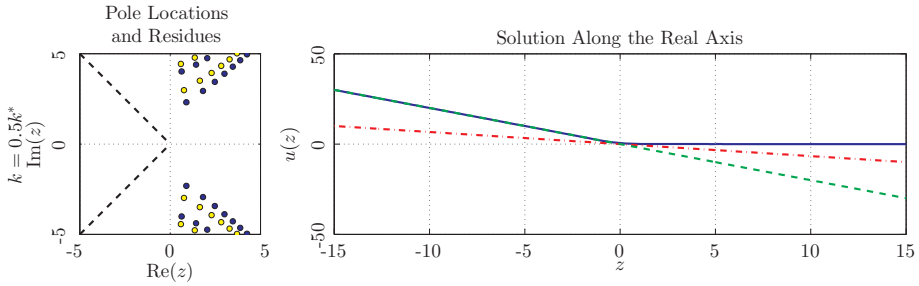

Figure 9: Solution to (6) with $\nu = -\frac{1}{2}$ and $k = 0.5k^*$. The dashed (black) lines on the left indicate the rays $re^{\pm i\frac{3\pi}{4}}$, $r \geq 0$. The dashed-dotted (red) and dashed (green) lines on the right show $-\frac{2}{3}z$ and $-2z$, respectively.

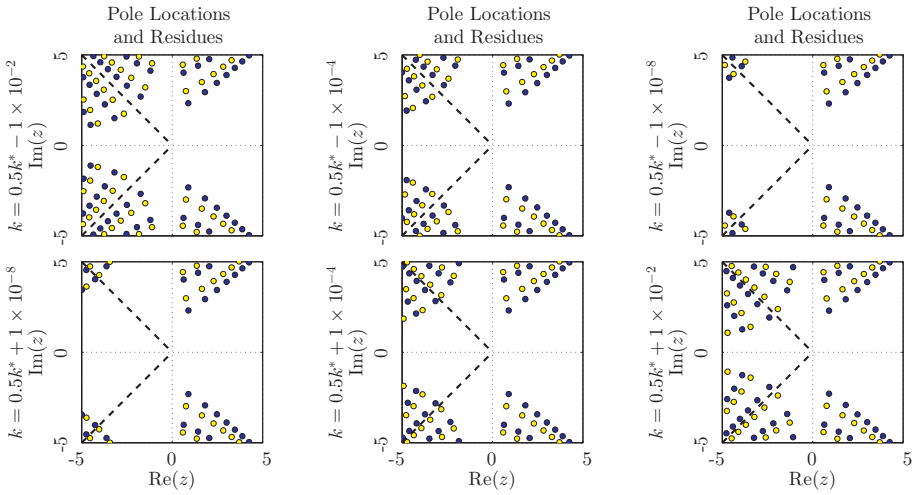

Figure 10: Solutions in the complex plane to (6) with $\nu = -\frac{1}{2}$ for six k-values near $k = \frac{1}{2}k^*$. The dashed (black) lines indicate the rays $re^{\pm i\frac{3\pi}{4}}$, $r \geq 0$.

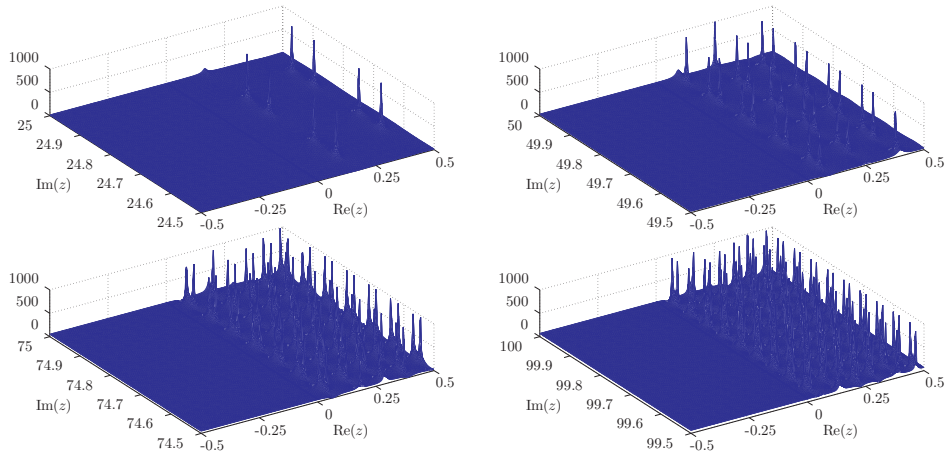

Figure 11: Solutions in the complex plane to (6) with $\nu = -\frac{1}{2}$ and $k = \frac{1}{2}k^*$. Here we show $|u(z)|$. That is we show pole locations only, without the alternating pattern of residues.

The pole free nature of the left half-plane and a large portion of the right half-plane is reminiscent of a special solution to P_I known as the tritronquée solution (see, for example,

[21], [10] or [14]). It is well known that the P_I equation,

$$\frac{d^2}{dz^2}u(z) \quad = \quad 6u(z)^2 + z, \tag{18}$$

is invariant under the changes $u \to \omega^3 u$, $z \to \omega z$ when $\omega^5 = 1$ (see, for example, [10]). This results in solutions with poles aligned in the five distinct sectors shown the left in figure 12. The tritronquée solution for P_I is pole free except for the region 1 in the figure, leaving the entire left half-plane pole free. Similarly, many of the P_{IV} solutions considered here indicate that the poles line up in the eight sectors shown to the right in figure 12. This will become even more apparent in section 4.6.

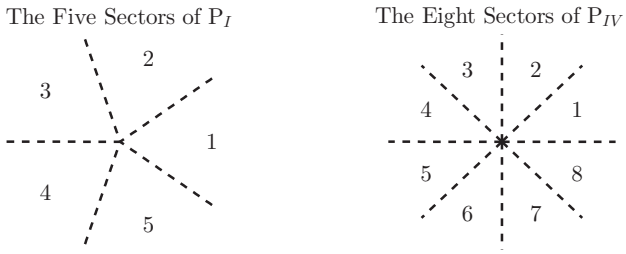

Figure 12: The asymptotic far field sector structures for the P_I and P_{IV} equations.

4.4 Tronquée-Like Solutions

In both the k-positive and k-negative cases behavior different from the tronquée solutions for P_I discussed in, for example, [10] and [14] is encountered. Concerning P_I, transitioning through tronquée initial data leads to a fundamental change in the location of the poles in the solutions. That is, beginning with a solution to P_I with no poles on the real axis, the initial conditions on the other side of the tronquée initial data will have poles on the real axis. The opposite occurs when beginning with poles on the real axis. Tronquée-like behavior for P_{IV} occurs at the transition from a shaded region in figure 2 to a blank region.

One of the tronquée-like solutions occurs when $u(0) \approx -1.59610846592044$ and $u'(0) = 1$. Figure 13 displays the behavior just described. Notice, also, that as $z \to \infty$ the solution at the critical initial data is asymptotic to $-2z$. This is found to be the case for nearly all tronquée-like solutions. The exception is the trivial solution when $u(0) = u'(0) = 0$.

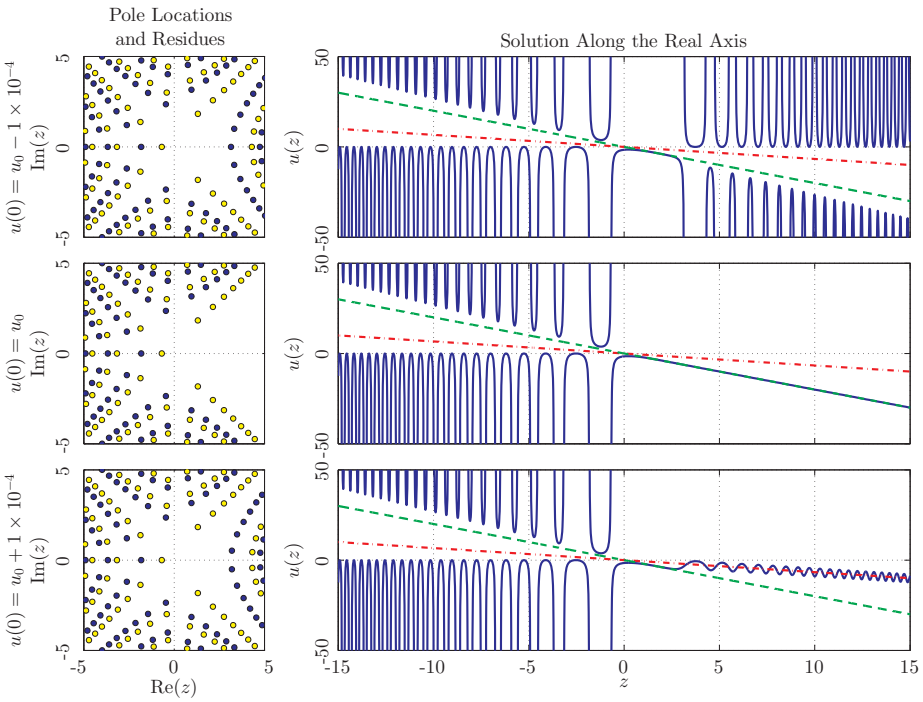

Figure 13: Solutions to (1) with $\alpha = \beta = 0$ and ICs $u_0 = -1.59610846592044$ and $u'(0) = 1$.

4.5 Solutions with a Pole at the Origin

Until now solutions have only been considered for which $u(0)$ and $u'(0)$ are finite. However, beginning with a truncated series like (2), with $z_0 = 0$, initial conditions can be generated to also view solutions with a pole at the origin. In the case of $\alpha = \beta = 0$ the expansion becomes

$$\begin{aligned} u(z) \quad \approx \quad & \pm\frac{1}{z} - \frac{4}{3}z + cz^2 \pm \frac{26}{45}z^3 \mp cz^4 + \frac{1}{945}\left(-128 \pm 405c^2\right)z^5 + \frac{41}{90}cz^6 + \\ & \frac{\left(\pm 1604 - 12960c^2\right)}{28350}z^7 + \frac{\left(\mp 3092 + 1800c^2\right)}{12600}cz^8 + \frac{\left(-10240 \pm 136512c^2\right)}{374220}z^9 + \\ & \frac{\left(45555 \mp 77760c^2\right)}{340200}cz^{10} + \frac{\left(\pm 15846104 - 324788400c^2 \pm 66156750c^4\right)}{1277025750}z^{11} + \\ & \frac{\left(\mp 27096717 + 92409660c^2\right)}{392931000}cz^{12} + O(z^{13}). \end{aligned} \tag{19}$$

Reiterating, the residue at the origin can be either $+1$ or -1, and the only remaining free parameter is c. Choosing $c = 0$ gives the two solutions shown in figure 14.

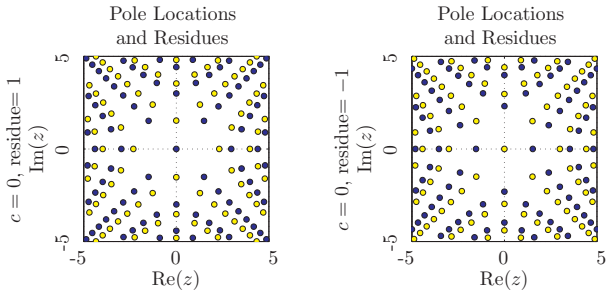

Figure 14: A view of solutions with a pole at the origin in the case of $c = 0$.

Varying $u(0)$ and $u'(0)$ allows the exploration of all solutions apart from those with a pole at the origin. In that case the single parameter c can instead be varied to explore the number of poles and oscillations along the two halves of the real axis. Figures 15 and 16 show that certain choices of c lead to solutions with a finite number of poles on the positive and negative real axes. This is shown in two ways for both possible choices of the residue for the pole located at the origin. On the left the locations of the poles on the real axis are shown, with solid lines indicating $+1$ residue and dashed lines indicating -1 residue. Due to (2) and (19) the curves are symmetric around the origin $\mathrm{Re}(z) = c = 0$. The right images mimic figure 2. In these images lines and dots correspond to values of c that generate solutions with a finite number of poles. The horizontal axis indicates the exact number of poles on either the positive or negative real axis. The corresponding half of the real axis is indicated by the color of the line or dot. Consequently, we can deduce that the colored and black dots indicate the values of c that correspond to solutions generated from (6) and (9) with $k > 0$ and $k < 0$, respectively. Colored line segments, then, correspond to colored regions in figure 2.

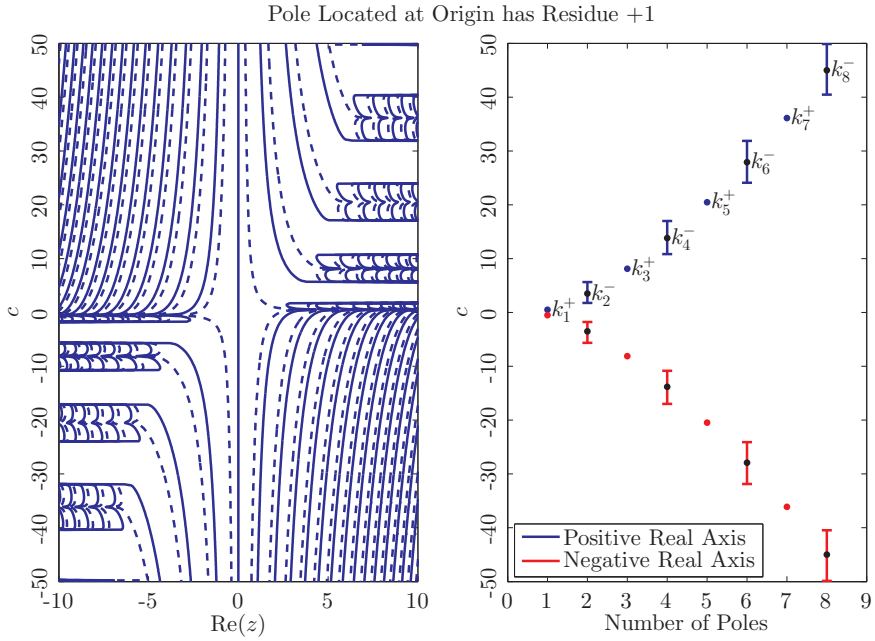

Figure 15: Left Frame: Locations of the poles on the real axis for various c. Solid lines indicate poles with residue $+1$ and dashed lines those with residue -1. Right Frame: Number of poles includes the pole at the origin. Values of c with no lines or dots indicate solutions with an infinity of poles on the real axis.

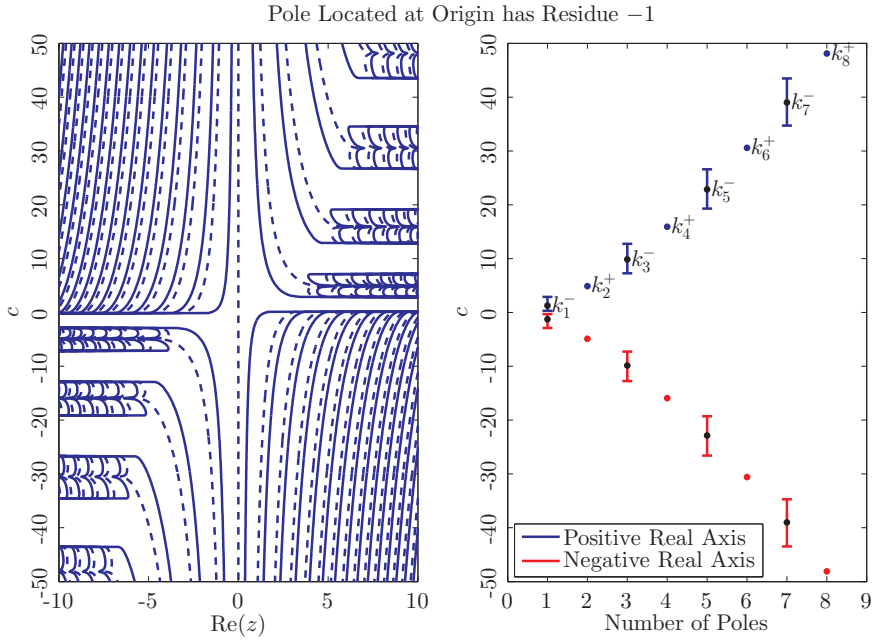

Figure 16: Left Frame: Locations of the poles on the real axis for various c. Solid lines indicate poles with residue $+1$ and dashed lines those with residue -1. Right Frame: Number of poles includes the pole at the origin. Values of c with no lines or dots indicate solutions with an infinity of poles on the real axis.

Table 1 shows the approximate values of k and c corresponding to the k_j^+ and k_j^-, $j = 1, 2, \ldots, 8$, solutions, respectively, in figures 4, 15 and 16. The columns ± 7.5 (out) and ± 7.5 (in) show the values of k where the dashed and solid line segments leave and enter the window in figure 4. The column labeled $\pm\infty$ gives the value of k corresponding to the transition of a pole through the origin. The c column and $\pm\infty$ column lead to the same solution when substituted into (19) and (9), respectively, to generate ICs.

Pole Located at Origin has Residue +1				
	k Corresponding to $u'(0)$ equal to			
	7.5 (out)	∞	7.5 (in)	c
k_1^+	0.87×10^0	1.54×10^0	3.49×10^0	0.5100
k_2^-	-6.82×10^1	-2.47×10^2	-1.42×10^3	3.5240
k_3^+	1.23×10^4	5.48×10^4	7.13×10^5	8.1000
k_4^-	-2.52×10^6	-1.25×10^7	-2.12×10^8	13.8100
k_5^+	5.50×10^8	2.85×10^9	5.75×10^{10}	20.4520
k_6^-	-1.22×10^{11}	-6.55×10^{11}	-1.45×10^{13}	27.9203
k_7^+	2.74×10^{13}	1.50×10^{14}	3.63×10^{15}	36.1202
k_8^-	-6.22×10^{15}	-3.45×10^{16}	-8.85×10^{17}	44.9203

Pole Located at Origin has Residue −1				
	k Corresponding to $u'(0)$ equal to			
	−7.5 (out)	$-\infty$	−7.5 (in)	c
k_1^-	-2.72×10^0	-6.97×10^0	-1.75×10^1	1.2710
k_2^+	2.69×10^2	1.49×10^3	5.34×10^3	4.9020
k_3^-	-2.97×10^4	-3.35×10^5	-1.42×10^6	9.8903
k_4^+	4.67×10^6	7.61×10^7	3.49×10^8	15.9233
k_5^-	-8.75×10^8	-1.75×10^{10}	-8.45×10^{10}	22.8524
k_6^+	1.77×10^{11}	4.00×10^{12}	2.02×10^{13}	30.5710
k_7^-	-3.75×10^{13}	-9.20×10^{14}	-4.77×10^{15}	38.3697
k_8^+	8.12×10^{15}	2.12×10^{17}	1.12×10^{18}	48.1000

Table 1: This table shows the approximate values of k and c corresponding to the k^+ and k^- solutions, respectively, in figures 4, 15 and 16. The columns ± 7.5 (out) and ± 7.5 (in) show the values of k where the dashed and solid line segments leave and enter the window in figure 4. The column labeled $\pm\infty$ gives the value of k corresponding to the transition of a pole through the origin. The c column and $\pm\infty$ column lead to the same solution when substituted into (19) and (9), respectively, to generate ICs.

In order to see how close the solutions corresponding to the $\pm\infty$ and c columns are, consider those for k_1^- in table 1. If the corresponding solutions are computed, the pole locations and residues are shown in figure 17. Notice that even these low precision values for k and c already lead to solutions that are very similar. The pole locations shared by both frames differ by at most $O(10^{-3})$.

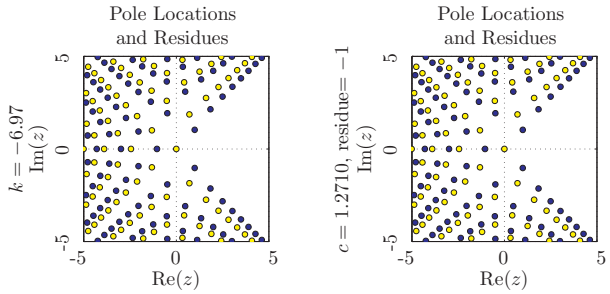

Figure 17: Solutions corresponding to the values in the $-\infty$ and c columns of k_1^- in table 1. Notice that even these low precision values lead to solutions that are very similar. The pole locations shared by both frames differ by at most $O(10^{-3})$.

4.6 Neighborhoods of Solutions

Throughout this paper several special solutions to P_{IV} with $\alpha = \beta = 0$ have been considered along with many of their neighboring solutions. However, the neighboring solutions that have been considered only resulted from a perturbation in the asymptotic parameter k or the single IC $u(0)$. To complete this study, consider six of the same special solutions, with the difference that now neighboring solutions that result from varying both $u(0)$ and $u'(0)$ are shown.

Figures 18, 19, 20, and 21 show solutions in the neighborhood of the middle row of each of the figures 5, 9, 6, and 7, respectively. The rays $re^{i\frac{j\pi}{4}}$, $r \geq 0$ and $j = 1, 2, \ldots, 8$, are included to highlight the behavior of the poles when the ICs are near or equal to those of a special solution. We find that near these particular ICs the poles fall within the eight distinct sectors discussed previously and shown in figure 12.

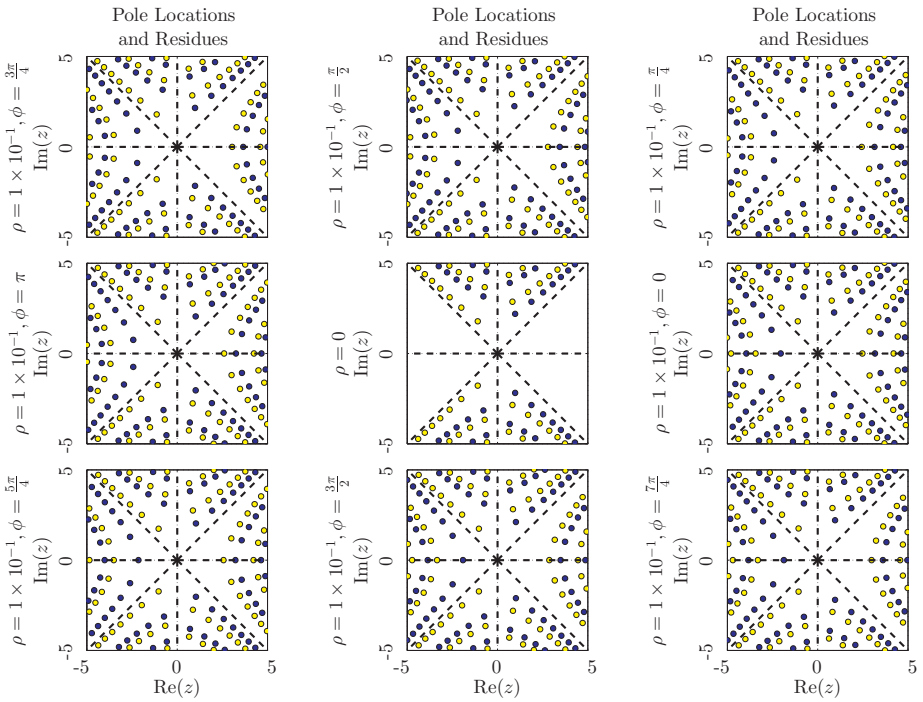

Figure 18: A view of the solutions with $u(0)$ and $u'(0)$ in a neighborhood of the values generated by (6) with ICs given by (9) where $\nu = -\frac{1}{2}$ and $k = k^*$ shown in figure 5. Here $u(0) = 0.555491078710868 + \rho\cos(\phi)$ and $u'(0) = -0.886725480333295 + \rho\sin(\phi)$ to generate the solutions.

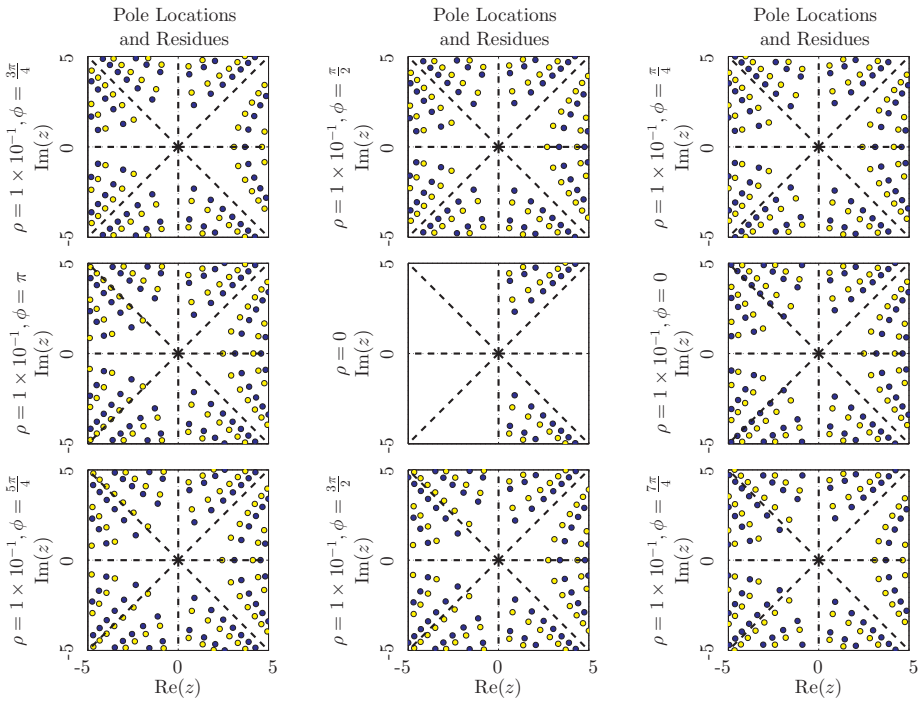

Figure 19: A view of the solutions with $u(0)$ and $u'(0)$ in a neighborhood of the values generated by (6) with ICs given by (9) where $\nu = -\frac{1}{2}$ and $k = \frac{1}{2}k^*$ shown in figure 9. Here $u(0) = 0.253975473568026 + \rho\cos(\phi)$ and $u'(0) = -0.367698229229807 + \rho\sin(\phi)$ to generate the solutions.

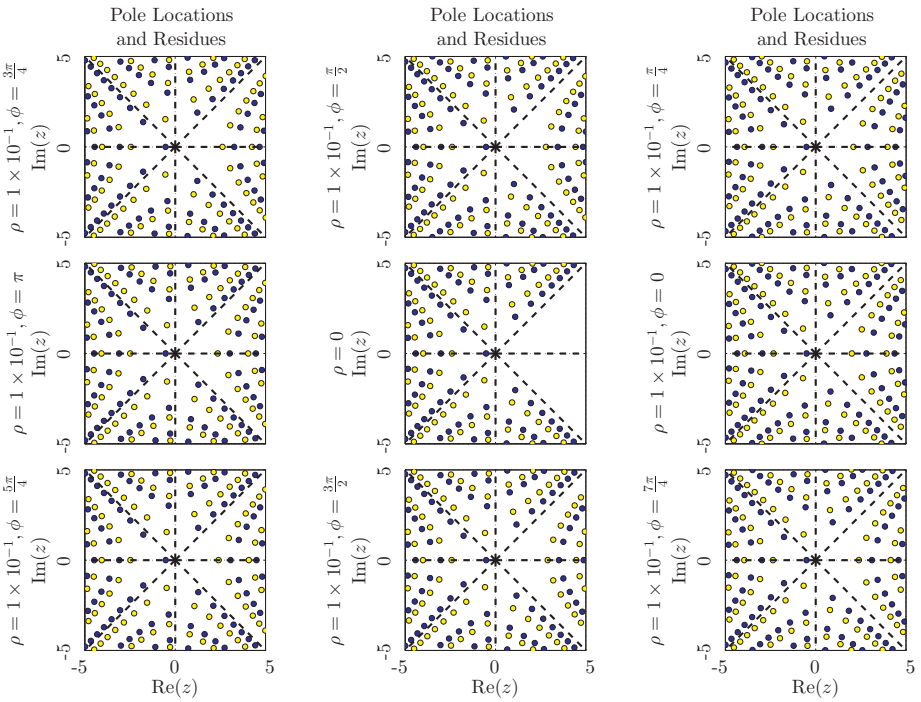

Figure 20: A view of the solutions with $u(0)$ and $u'(0)$ in a neighborhood of the values generated by (6) with ICs given by (9) where $\nu = -\frac{1}{2}$ and $k = 0.75$ shown in figure 6. Here $u(0) = 1.852476801971173 + \rho\cos(\phi)$ and $u'(0) = -4.634118664573674 + \rho\sin(\phi)$ to generate the solutions.

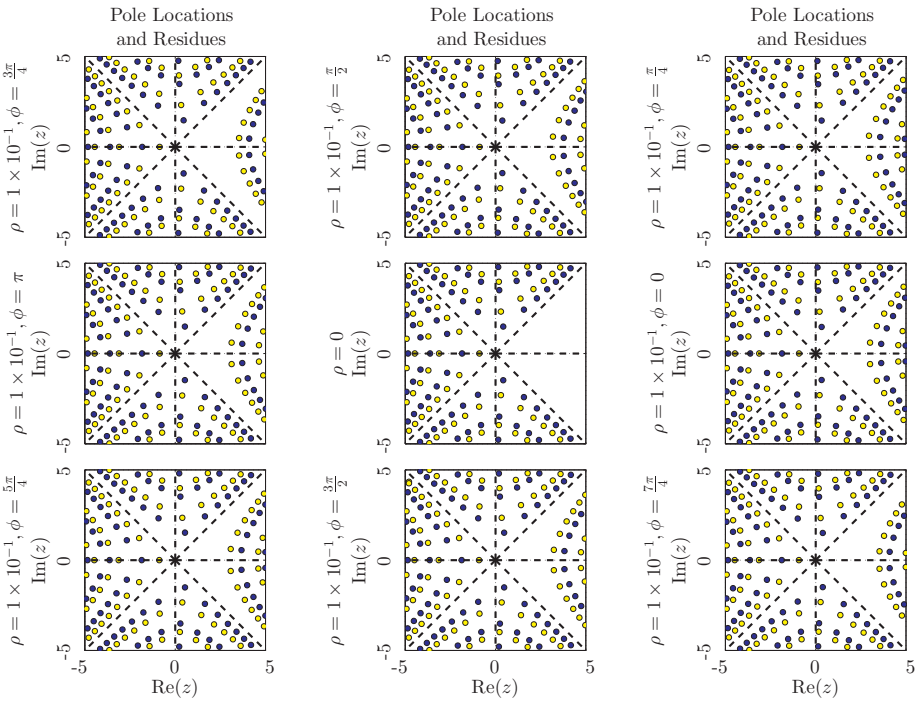

Figure 21: A view of the solutions with $u(0)$ and $u'(0)$ in a neighborhood of the values generated by (6) with ICs given by (9) where $\nu = -\frac{1}{2}$ and $k = -0.75$ shown in figure 7. Here $u(0) = -0.878189808443538 + \rho\cos(\phi)$ and $u'(0) = 1.142924661194064 + \rho\sin(\phi)$ to generate the solutions.

Solutions with initial conditions given in a neighborhood of the origin (figure 22) and near the tronquée-like solution (figure 23) shown in figure 13 are also displayed. Notice figures 2-4 show that when $u(0) = 0$ and $u'(0) \neq 0$ the solutions have pole fields of infinite density. Therefore, only six neighboring solutions around $u(0) = u'(0) = 0$ are given.

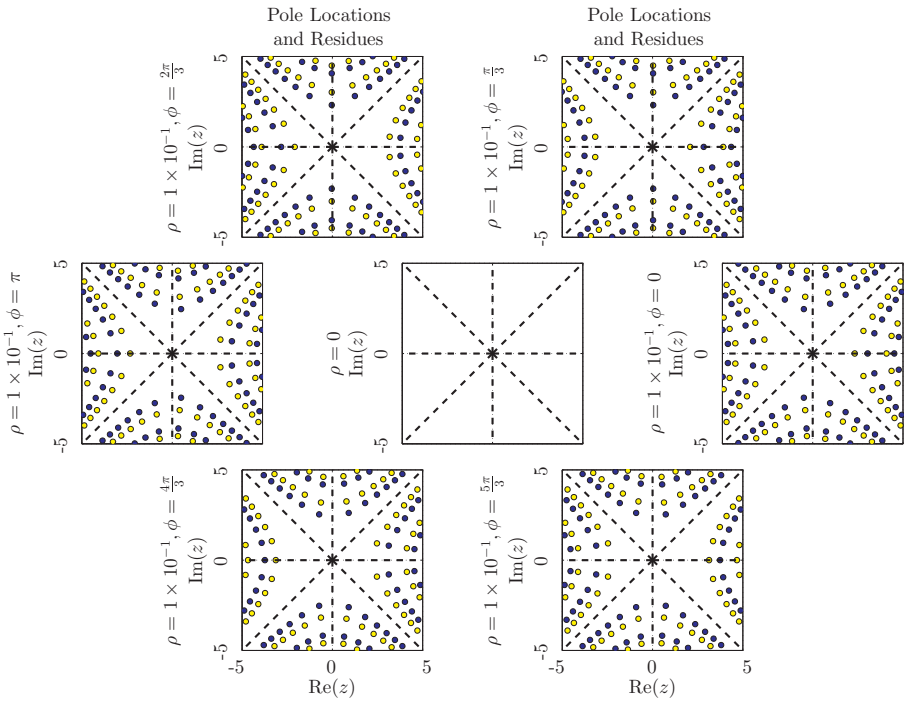

Figure 22: A view of the solutions in a neighborhood of the origin. Here $u(0) = \rho\cos(\phi)$ and $u'(0) = \rho\sin(\phi)$ to generate the solutions. Since we cannot compute numerically the solution when $u(0) = 0$, except when $u'(0) = 0$ also, we show only six neighboring solutions in a neighborhood of the origin to preserve symmetry.

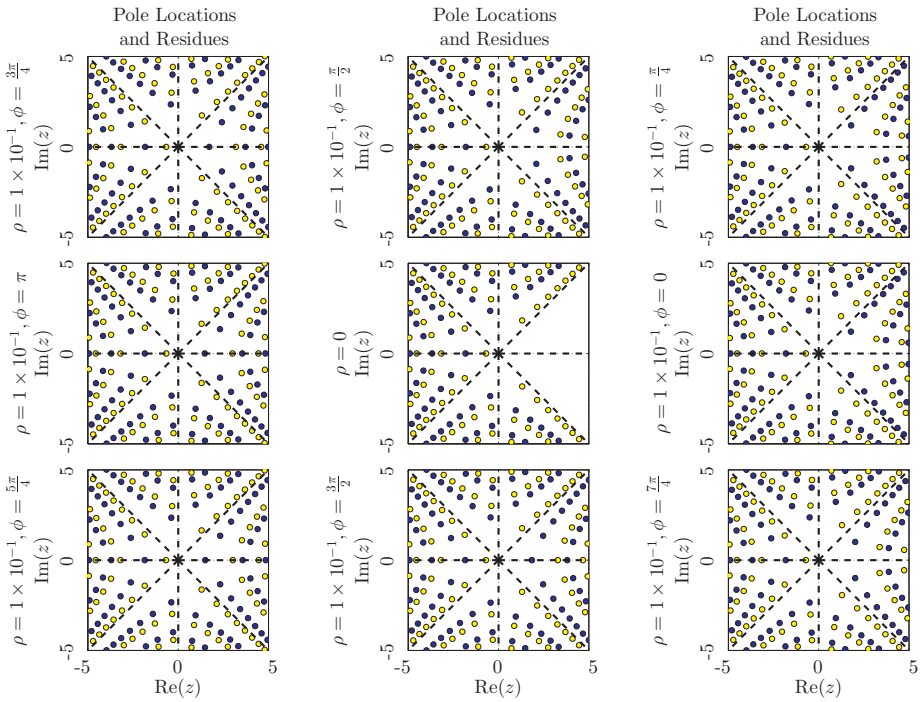

Figure 23: A view of the solutions in a neighborhood of the tronquée-like solution shown in 13. Here $u(0) = -1.59610846592044 + \rho\cos(\phi)$ and $u'(0) = 1 + \rho\sin(\phi)$ to generate the solutions.

5 Conclusions

In this study of the fourth Painlevé equation for the case $\alpha = \beta = 0$ (i.e. $\nu = -\frac{1}{2}$), existing analytic and asymptotic knowledge about the equation has been confirmed, and solution regimes which have not been described in the previous literature were explored. The fast numerical approach introduced in [10] allowed the location ICs with unique characteristics. Notably, a solution that has no poles located in the entire left half-plane was discovered. Likewise, symmetry leads to a solution that is pole free in the entire right half-plane.

This study has highlighted some peculiar behavior in the neighborhood of some of the known asymptotic solutions. Further, the existence of an entire family of solutions, like the one in figure 13, was confirmed that is similar to the tronquée solutions of P_I. Connections were also made between the free parameter, c, in the Laurent expansion of a pole located

at the origin and the asymptotic parameter k.

The flexibility of the numerical algorithm has left ample opportunities for further explorations of the solutions of P_{IV}, particularly for nonzero α and β. A few of these include:

- Confirmation of known rational and special function solutions, and exploration of solutions with neighboring ICs.
- Finding connections between parameter choices with known asymptotic and analytic solutions and neighboring parameter choices with no such information available.
- Locating yet unknown solutions with large pole free sectors in the complex plane.

References

[1] F. W. J. Olver, D. W. Lozier, C. W. Clark, and R. F. Boisvert. NIST Handbook of Mathematical Functions. Cambridge Univ. Press, Cambridge, 2010. http://dlmf.nist.gov/.

[2] M. Abromowitz and I. A. Stegun. Handbook of Mathematical Functions. Dover, New York, 1964.

[3] P. J. Forrester and N. S. Witte. Application of τ-function theory of Painlevé equations to random matrices: PIV, PII, and the GUE. Commun. Math. Phys. 219:357–398 (2001).

[4] E. Kanzieper. Replica field theories, Painlevé transcendents, and exact correlation functions. Phys. Rev. Lett. 89(25) (2002).

[5] V. A. Osipov and E. Kanzieper. Correlations of RMT characteristic polynomials and integrability: Hermitian matrices. Annals of Physics 325(10):2251–2306 (2010).

[6] C. Tracy and H. Widom. Fredholm determinants, differential equations and matrix models. Commun. Math. Phys. 163(1):33–72 (1994).

[7] D. Bermúdez and D. Fernández. Solution hierarchies for the Painlevé iv equation. In Proceedings of the XXXI Workshop on Geometric Methods in Physics, Bialowieza, Poland, June 2012.

[8] P. A. Clarkson. The fourth Painlevé equation and associated special polynomials. Journal of Math. Physics 44(11):5350–5374 (2003).

[9] A. P. Bassom, P. A. Clarkson, and A. C. Hicks. Numerical studies of the fourth Painlevé equation. IMA Journal of Applied Mathematics 50:167–193 (1993).

[10] B. Fornberg and J. A. C. Weideman. A numerical methodology for the Painlevé equations. Journal of Computational Physics 230:5957–5973 (2011).

[11] I. M. Willers. A new integration algorithm for ordinary differential equations based on continued fraction approximations. Comm. ACM 17:504–508 (1974).

[12] B. Fornberg and J. A. C. Weideman. A computational study of the second Painlevé equation. in preparation, 2012.

[13] V. I. Gromak, I. Laine, and S. Shimomura. Painlevé Differential Equations in the Complex Plane. Walter de Gruyter, Berlin, 2002.

[14] V. Y. Novokshenov. Padé approximations for Painlevé I and II transcendants. Theor. and Math. Phys. 159(3):853–862 (2009).

[15] S. Olver. A general framework for solving Riemann-Hilbert problems numerically. Numer. Math (2012). DOI 10.1007/s00211-012-0459-7.

[16] P. A. Clarkson. The fourth Painlevé transcendent. Technical Report UNK, Institute of Mathematics, Statistics and Actuarial Science, University of Kent, November 2008.

[17] A. R. Its and A. A. Kapaev. Connection formulae for the fourth Painlevé transcendent: Clarkson-McLeod solution. J. Phys. A: Math. Gen. 31:4073–4113 (1998).

[18] A. P. Bassom, P. A. Clarkson, A. C. Hicks, and J. B. McLeod. Integral equations and exact solutions of the fourth Painlevé equation. Proc. R. Soc. Lond., Ser. A 437:1–24 (1992).

[19] P. A. Clarkson and J. B. McLeod. Painlevé Transcendents, their Asymptotics and Physical Applications. Plenum, New York, 1992.

[20] C. M. Bender and S. A. Orszag. Advanced Methods for Scientists and Engineers. McGraw-Hill, New York, 1978.

[21] P. Boutroux. Recherches sur les transcendents de M. Painlevé et l'étude asymptotique des équations différentielles du second ordre. Ann. École Norm. Sup. 30(3):255–375 (1913).